

Is Spillover Relevant for Hydrogen Adsorption and Storage in Porous Carbons Doped with Palladium Nanoparticles?

María Blanco-Rey,^{*,†,‡} J. Iñaki Juaristi,^{†,¶,‡} Maite Alducin,^{¶,‡} María J. López,[§]
and Julio A. Alonso^{*,§,‡}

[†] *Departamento de Física de Materiales, Facultad de Químicas UPV/EHU, Apartado 1072,
20080 Donostia-San Sebastián, Spain*

[‡] *Donostia International Physics Center (DIPC), Paseo Manuel de Lardizabal 4, 20018
Donostia-San Sebastián, Spain*

[¶] *Centro de Física de Materiales CFM/MPC (CSIC-UPV/EHU), Paseo Manuel de
Lardizabal 5, 20018 Donostia-San Sebastián, Spain*

[§] *Departamento de Física Teórica, Atómica y Óptica, Universidad de Valladolid, 47011
Valladolid, Spain*

E-mail: maria.blanco@ehu.es; jaalonso@fta.uva.es

Phone: +34 943015366; +34 983423142

Abstract

Experiments have shown that the efficiency of nanoporous carbons to store hydrogen becomes enhanced by doping the material with metallic nanoparticles. In particular, doping with palladium has been used with success. The hypothesis to justify the enhancement has been that the Pd nanoparticles dissociate the hydrogen molecules and then the hydrogen atoms spill over the carbon substrate, where the hydrogen is retained. To test this hypothesis we have performed ab initio molecular dynamics simulations of the deposition of molecular hydrogen on Pd nanoparticles (Pd_6 and Pd_{13}) supported on graphene, which is a good model for the wall of a carbon nanopore. Three channels have been identified in the simulations: bouncing off the molecule, molecular adsorption, and dissociation of the molecule in two H atoms. The relative percentage of those channels is sensitive to the size of the Pd particle. Dissociation occurs more frequently on Pd_{13} and it generally takes place on the lateral regions of the Pd particles. However, in our simulations we have not found a single case of H atoms or H_2 molecules spilling over the carbon substrate. We have also tested the situation when several H atoms are preadsorbed on the Pd_6 and Pd_{13} particles and found that not a single dissociation event occurs on these H-saturated nanoparticles. These results lead us to cast strong doubts on the validity of the spillover mechanism for explaining the enhancement of hydrogen adsorption on porous carbons doped with transition metal nanoparticles.

1 Introduction

The technology of hydrogen fuel cells is well developed.¹ However, the main difficulty preventing a widespread use of hydrogen as an alternative fuel in cars is the efficient storage of hydrogen on board.² The only method available at present consists in storing hydrogen gas at high pressure (about 700 atm.) in a metallic container. This is an important advance, but the opinion of many scientists and engineers is that it is not the ultimate solution. For this reason, other storage technologies are being investigated and one that is receiving much attention is the storage in porous materials. Several families of porous materials have been studied for this purpose: porous carbons,^{3,4} metal organic frameworks,⁵ zeolites,⁶ clathrate hydrates,⁷ and microporous organic polymers.⁸ Targets to be achieved in the short term (year 2020) are 5.5 per cent of hydrogen in weight and a volumetric capacity of 40 grams of hydrogen per liter at room temperature and moderate pressures, with ultimate targets of 7.5 per cent in weight and 70 grams per liter.⁹

Focusing on the porous carbons, there is experimental¹⁰⁻¹² and theoretical evidence^{4,13-17} that hydrogen storage on clean porous carbon materials does not fulfill the recommended targets. However, a number of experiments indicate that doping porous carbon materials (nanotubes, nanofibers, nanoporous carbons) with metallic clusters or nanoparticles could provide a strategy to increase the hydrogen uptake.¹⁸⁻²⁶ The metals mostly used in those investigations are alkali metals^{18,19} and some transition metals like vanadium, palladium, and platinum.²²⁻²⁷ To explain the observed enhancement of the hydrogen adsorption, a mechanism of spillover^{28,29} has generally been assumed.^{22-27,30,31} In that mechanism, the hydrogen molecules are first adsorbed and dissociated on the surface of the metallic nanoparticles, and are next transported onto the surface of the substrate carbon material. However, in our opinion, the validity of that spillover idea has not been scrutinized critically.

To get insight into the spillover process we have performed (microcanonical) ab initio molecular dynamics (AIMD) simulations of the deposition of hydrogen molecules on a substrate formed by palladium clusters supported on a graphene layer, using density functional

theory (DFT). The graphene layer is a good model for the wall of the pores in nanoporous carbons.³² The molecules are dropped from a certain distance above the cluster with a given kinetic energy and their classical dynamical evolution is followed as they interact with the substrate. In a fraction of the studied simulations the deposited H₂ molecules experience catalytic dissociation in two hydrogen atoms, and by comparing the results for two different Pd clusters, Pd₆ and Pd₁₃, insight is gained on the influence of cluster size. We also find that H atoms preadsorbed in the clusters, which have been proposed in the literature as spillover promoters,³³ hinder dissociation. Both the H₂ molecules and the H atoms wander around on the surface of the Pd cluster, but mass transfer to the carbon substrate was not observed in any of the studied cases. The number of simulations performed is sufficiently large to let us conclude that the idea of a mechanism of spillover to explain the enhancement in hydrogen adsorption in graphene doped with palladium nanoparticles should be taken with care. In other words, spillover should not be taken for granted when modelling hydrogen uptake in porous carbon doped with transition metal nanoparticles, and we suggest that specific experiments testing the mechanism in depth should be performed.

The paper is organized as follows. In section 2 we explain the calculation details. The results for clean Pd nanoparticles and for Pd nanoparticles with preadsorbed H are, respectively, shown and discussed in sections 3.1 and 3.2. Finally, in section 4 we summarize the main results and give the conclusions of this work.

2 Computational details

The AIMD calculations are performed with the “Vienna ab initio simulation program” (VASP),^{34,35} which is based on DFT. The exchange–correlation energy is calculated within the generalized gradient approximation (GGA) using the PW91 functional.³⁶ All the calculations allow for spin polarization of the system. The electron-core interaction is treated in the projector augmented wave (PAW) approximation.³⁷ The Brillouin zone integration is

performed with a Γ -centered $2 \times 2 \times 1$ Monkhorst-Pack grid of special k-points.³⁸ The energy cut-off used in the plane-wave basis set is 400 eV. Fractional occupancies are determined through the Methfessel-Paxton broadening scheme of first order using a width of 0.1 eV.³⁹ The convergence criterion for total energy self-consistency in each ionic step is 10^{-5} eV. The calculations have been performed with periodic boundary conditions using appropriate supercell sizes. In the case of the Pd₆ nanoparticle, the supercell consists in a hexagonal 5×5 graphene layer in the lateral directions, which corresponds to a supercell lattice parameter of 12.33 Å. In the direction normal to the graphene layer the height of the supercell is 14 Å. The most stable structure of isolated Pd₆ is an octahedron, and this structure is preserved for Pd₆ supported on graphene, with a triangular face of the octahedron lying on the graphene layer.⁴⁰ In that structure, the supported Pd₆ cluster can be viewed as formed by two parallel triangular layers, being the lower one in contact with the graphene surface. The magnetic moment, $2 \mu_B$, of the free Pd₆ cluster is preserved upon deposition on the graphene layer. However the dissociative adsorption of hydrogen quenches the moment of the cluster down to zero.⁴⁰⁻⁴² In the case of the Pd₁₃ nanoparticle, the supercell consists in a hexagonal 6×6 graphene layer in the lateral directions, which corresponds to a supercell lattice parameter of 14.80 Å. The length of the supercell in the direction normal to the graphene layer is again 14 Å. The ground state structure of both the free and the supported Pd₁₃ nanoparticles consists in two (111) *fcc* planes with seven and six atoms, respectively. For the deposited particle, the face with seven atoms rests on the graphene layer. The magnetic moment, $6 \mu_B$, of the free Pd₁₃ cluster is reduced to $4 \mu_B$ upon deposition on the graphene layer. The dissociative adsorption of one hydrogen molecule quenches further the moment of the cluster down to $2 \mu_B$ and finally additional adsorption of hydrogen cancels the moment. To better understand some of the results of the dynamical simulations, we have also investigated the dissociation barriers, through calculations of the minimum energy path (MEP) for hydrogen dissociation and of the equilibrium configurations where hydrogen is located on the graphene layer near the Pd nanoparticles. These calculations are performed with the Dacapo code,⁴³

which is a DFT code that uses Vanderbilt ultrasoft pseudopotentials⁴⁴ to describe the interaction between the valence electrons and the ionic cores. A basis set of plane waves is used to expand the electronic wave functions and density, with cutoff values of 500 eV and 1000 eV, respectively. We have used the same (PW91) exchange correlation functional as in the AIMD calculations. Similar equilibrium configurations and adsorption energies are obtained from VASP and Dacapo calculations. The small differences in the relaxed atomic positions and energies can be quantified with the following representative test on the supported clean Pd₁₃ nanoparticle: we find full agreement between the geometries optimized with Dacapo and VASP, with differences in the atomic positions smaller than 0.10 Å. The energy difference between those structures, calculated with VASP, is 0.056 eV. Moreover, the hydrogen dissociation energies on the supported Pd₁₃ calculated with the two codes agree within 50 meV.

The initial translational energy E_i of the H₂ molecules in the AIMD simulations is 0.125 eV and their vibrational energy is that corresponding to the vibrational zero point energy (0.27 eV). The incidence direction is normal to the graphene layer and the simulations begin with the molecules located at a height of $Z = 9$ Å above the graphene layer, where the interaction of the molecule with both the graphene layer and the Pd nanoparticle is negligible (the forces on H₂ are below 3 meV/Å). A random sampling of the initial lateral positions (X, Y) and orientations of the molecules has been performed in a restricted triangular area around the nanoparticle position (see Fig. 1). This area has been selected in order to minimize the interaction between the H₂ molecules and the clean graphene regions, not relevant to the present study. Before starting the dynamical simulations the substrate is relaxed until the Pd and C atoms reach their equilibrium positions (for each atom the forces are below 0.01 eV/Å). Along the dynamics, all the atomic degrees of freedom are free and the hydrogen and substrate atoms are allowed to move according to the forces acting on them. All the trajectories are run for 1 ps with a time step of 0.5 fs, which allows for a satisfactory conservation of the energy during the simulation. Specifically, the energy drift ΔE is below

12 meV in all cases except for a few dissociated trajectories in Pd₆ for which $\Delta E < 30$ meV. Sixty different trajectories are simulated for each nanoparticle, the different trajectories corresponding to different initial positions and orientations of the H₂ molecule. As outcome of the trajectory simulations we distinguish the following events: (i) dissociation of the H₂ molecule, (ii) non-dissociative molecular adsorption, and (iii) reflection (non-reactive scattering). A dissociation event is considered when the internuclear distance between the two atoms of the H₂ molecule is larger than 1.6 Å. The molecular adsorption channel corresponds to those molecules that at the end of the simulation, after 1 ps, remain non-dissociated and moving around the Pd nanoparticles at distances from their center not larger than 4.5 Å for Pd₆ and 5.5 Å for Pd₁₃. Two different kinds of trajectories are included in the reflection channel. On the one hand, we consider as reflected molecules those that, after being scattered off the nanoparticle, reach the height $Z = 8.5$ Å with a positive Z -component of the velocity. On the other hand, there exist some trajectories in which the molecules are scattered off the Pd nanoparticle with a small normal velocity. These molecules arrive at the boundaries of the simulation cell and interact with a periodic image of the initial nanoparticle, as a result of using periodic boundary conditions. In our analysis we have considered these trajectories as reflected. Finally, only in a few cases pathological trajectories exist that have an unclear outcome and thus they are excluded from the analysis.

3 Results and Discussion

3.1 H₂ incident on clean Pd nanoparticles supported on a graphene layer

We start this section by analyzing the AIMD results performed on the clean Pd₆ and Pd₁₃ nanoparticles supported on a graphene layer. Table 1 shows the number of trajectories in each final channel (dissociation, molecular adsorption, and reflection) for these nanoparticles. The number of reflected molecules is similar in both Pd₆ and Pd₁₃. However, the relative

proportion of adsorbed and dissociated molecules is very different. In the case of Pd₁₃ most of the molecules that are adsorbed dissociate, whereas dissociation is much reduced on Pd₆. We note that the molecule initial position within the triangular sampling area does not seem to dictate the outcome of the trajectory. This can be observed in Fig. 1, where the initial positions are identified attending to the different outcomes. A detailed inspection of the trajectories shows that most of the dissociation events occurring on both nanoparticles are direct and fast. Figure 2 shows the snapshots of two representative trajectories leading to dissociation on the Pd₆ and Pd₁₃ nanoparticles. As shown in this figure, the H₂ molecule, once it interacts with the nanoparticle, first orients itself with the molecular axis lying on a Pd atom of the top layer, leaning then towards the lateral side of the nanoparticle where it rapidly dissociates. The resulting H atoms wander around the external walls of the nanoparticle and occasionally penetrate inside the nanoparticle and then move again to the surface. Finally, though the Pd atoms are displaced from their equilibrium positions upon interaction with the impinging molecule, we observe that the subsequent deformation of the Pd nanoparticles is minor and that they basically keep their original structure intact.

Since Pd₁₃ is expected to be more rigid than Pd₆, it may seem surprising that H₂ dissociation is more probable in the former than in the latter. In order to understand this fact, we have compared the barriers to dissociation in the two systems. The energetics for the dissociation of H₂ on Pd₄, Pd₅ and Pd₆ supported on graphene has been already presented in ref. 40. Here, we have extended this analysis calculating the MEP for H₂ dissociation on supported Pd₁₃. First we notice that the molecular adsorption of hydrogen takes place without activation barrier and that the preferential adsorption sites are on the Pd atoms of the upper layer. On the other hand, the dynamical simulations show that the dissociation of the hydrogen molecules takes place preferentially on the lateral faces of Pd₁₃. Therefore, we have generated a MEP between two fixed relevant configurations, the first one corresponding to the hydrogen molecule adsorbed on a lateral Pd atom of the upper layer of the cluster and the other corresponding to the dissociated molecule with the H atoms adsorbed on two

non-adjacent lateral faces of Pd₁₃. The H-H distance $d(\text{H-H})$ is taken as the reaction coordinate and the configurations along the path are obtained through constrained minimizations of structures intermediate between those of the extreme points. Constrained minimization means that the positions of the H and Pd atoms are relaxed, keeping fixed the $d(\text{H-H})$ value. Figure 3 shows the energies and some structures along the MEP. Starting with the hydrogen molecule adsorbed onto a Pd atom of the upper layer (a), the molecule leans towards one Pd-Pd bond (b). One of the H atoms, the first, attaches to that bond, weakening the H-H bond, and the other H atom, the second, separates from the first one (c). The first H moves towards a lateral face (d) and the second H attaches to a Pd-Pd bond (e). Then, the two H atoms move towards their respective final configurations adsorbed above two non-adjacent lateral faces of the Pd cluster (f). The energy barrier for dissociation along this path is of 29 meV. This sets an upper limit for the dissociation barrier on Pd₁₃.

The dissociation barriers of H₂ on supported Pd₄, Pd₅, Pd₆ and Pd₁₃ are 0.46, 0.26, 0.30 and 0.03 eV, respectively (the dissociation barrier for Pd₆ is also shown in Fig. 3). A tendency for the height of the dissociation barrier to decrease as the size of the Pd cluster increases is evident. In fact, the barrier for dissociation on Pd₁₃ is quite small, and this low value is the reason for H₂ dissociation to be more favorable on this cluster. Notice also that, measured with respect to the molecule in the gas phase, there is no barrier to dissociation (the same happens for Pd₆). However, the dynamical simulations show that the absence of energy barriers does not mean that all the molecules dissociate. As a matter of fact, the probabilities for dissociation amount to just about 33% in the Pd₁₃ nanoparticle and only to 5% in Pd₆. The reason is that a large amount of the molecules do not find the most favorable path to dissociation and are either reflected or molecularly adsorbed.

In order to characterize better the dynamical aspects of the interaction, we have analyzed the evolution of $d(\text{H-H})$ and of the distortions caused in the Pd clusters. The $d(\text{H-H})$ values are shown as a function of time in Fig. 4 for each of the three channels. Those internuclear distances have been averaged over the number of trajectories of each channel for the Pd₆

and Pd₁₃ nanoparticles. In the case of the trajectories in which the hydrogen molecule reaches the cell boundary, included in the reflection channel, the simulations are stopped when the distance between the molecule and the center of the images is 5.5 Å for Pd₁₃ and 4.5 Å for Pd₆, i.e., before the interactions with the adjacent nanoparticles are effective. The figure clearly demonstrates the validity of the criterion that we have chosen to define H₂ dissociation: while the d(H-H) values rapidly increase above 1 Å for the dissociated H₂, they remain around the equilibrium bondlength in the other two channels. Additionally, the figure allows us to establish the typical time needed for the direct dissociation, which is around 100 fs for Pd₁₃ and around 200 fs for Pd₆. Only in the case of Pd₁₃ we find one trajectory in which dissociation takes place after being molecularly adsorbed for nearly 1 ps.

The average displacements of the Pd atoms in the Pd₆ and Pd₁₃ particles upon their interaction with the incoming molecule are shown as a function of time in Fig. 5 for the different outcome channels. For both nanoparticles, those displacements are relatively large in the case of the dissociating molecules. The reason for this is the great exothermicity of the process, similar in both cases (the released dissociation energy on Pd₆ and Pd₁₃ is of 1.2 and 1.4 eV, respectively), which requires that the energy liberated in the dissociation is transferred to the substrate atoms. Clear differences between the two nanoparticles are observed for the molecular adsorption events. While the Pd displacements are small in Pd₁₃, and similar to those occurring in the case of H₂ reflection, the displacements caused by the molecular adsorption mechanism in Pd₆ are large and comparable to those observed for dissociation. These results show that, indeed, the larger particle is more rigid. Furthermore, we have observed that in four trajectories of the molecular adsorption channel on Pd₆ the nanoparticle rotates over itself and ends up sitting on an edge over the graphene layer instead of lying on a face. The contribution to the averaged displacements from those trajectories is relatively large (see Fig. 5).

An important result is that none of our dynamical simulations shows transfer of hydrogen atoms to the underlying graphene layer that could support the idea of the spillover process.

This conclusion does not depend on the size of the Pd cluster since it is obtained for both supported Pd₆ and Pd₁₃. This is neither the result of the incidence conditions imposed to the molecules in the simulations. We have also performed additional simulations with an incident energy of 0.250 eV for the Pd₁₃ nanoparticle that show, not only a total absence of H transfer to the graphene layer, but also that the adsorption probability in the nanoparticle is reduced from 37 % to 23 %. Since H₂ dissociation takes place very fast (during the first 100-200 fs), it looks extremely unlikely that the hydrogen atoms may travel to the graphene layer at times longer than the simulation times of 1 ps. Although variations of either the molecule orientation or the incidence angle can vary the adsorption probabilities for a given incident energy, the memory of the initial conditions is lost soon after collision with the nanoparticle, which rules them out, too, as relevant factors in spillover. Eventual mechanisms may exist that, being characterized by reaction paths involving very reduced regions of the configurational space, would require longer times. Nonetheless, energy dissipation effects also active at longer times would make spillover very improbable. A similar outcome occurs for the simulations leading to molecular adsorption. Also the molecules stay adsorbed on the Pd nanoparticles with no sign of spilling over the carbon substrate.

3.2 H₂ incident on H-covered Pd nanoparticles supported on a graphene layer

It has been suggested that the presence of preadsorbed hydrogen on the nanoparticle may facilitate the dissociation of additional H₂,⁴⁵⁻⁴⁸ and that the spillover mechanism may be more effective in Pd nanoparticles initially saturated with atomic hydrogen.³¹ In order to analyze those hypotheses we have also performed AIMD simulations for H₂ molecules incident on a supported Pd₆ particle with six preadsorbed H atoms (Pd₆H₆) and a Pd₁₃ particle with 12 preadsorbed H atoms (Pd₁₃H₁₂). The equilibrium positions of the preadsorbed H have been determined from additional static DFT calculations by analysing the energetics of the covered clusters. In the case of Pd₆H₆, the six hydrogen atoms are located in the

equilibrium adsorption sites in the lateral walls of the nanoparticle (see Fig. 6(a)). In this way, only one adsorption site is left vacant at the top of the nanoparticle. In the case of the Pd₁₃, we find that up to seven H₂ molecules can be dissociatively adsorbed in the cluster. Therefore, in order to have free adsorption sites for the incoming H₂, we have performed simulations on Pd₁₃ covered with 12 preadsorbed H atoms. In the most stable structure with this stoichiometry the H atoms are adsorbed in the hollow sites leaving nonadjacent vacancies (see Fig. 6(b)). By choosing these structures as the starting condition for our AIMD simulations, we maximize the coverage in each case and, in principle, the chances for spillover. The results of the AIMD simulations for these nanoparticles are also summarized in Table 1. The number of reflection events is similar to the numbers obtained in the clean Pd₆ and Pd₁₃ nanoparticles. However, in contrast to them, no dissociation events occur on the Pd₆H₆ and the Pd₁₃H₁₂ nanoparticles since all the adsorbed molecules remain non-dissociated. Definitely, the presence of preadsorbed atomic hydrogen on the metallic nanoparticle complicates the dissociation of molecular hydrogen impinging on the nanoparticle. Also in contrast to the Pd₆ and Pd₁₃ cases, we find that the H-covered nanoclusters can be significantly altered upon interaction with the incoming H₂. As shown in Fig. 5, the Pd atoms are subject to much larger displacements. In particular, the structure of the Pd₆H₆ gets sometimes appreciably distorted due to the breaking of some Pd-Pd and Pd-C bonds (see Fig. 6(c)). In the Pd₁₃H₁₂ nanoparticle, the Pd-C bonds are also softened upon interaction with the incoming H₂. However, in this case, instead of inducing deformation of the nanoparticle, this softening of the bonds leads to a displacement of the nanoparticle over the graphene layer of around 0.6 Å (see Fig. 6(d)). As a final remark, note that in spite of all these differences between the results obtained for the clean and covered nanoparticles, no transfer of hydrogen (neither molecular nor atomic) towards the graphene layer is observed in any of the cases under study.

The fact that spillover is not observed in the DFT simulations is supported by an analysis of the energies corresponding to the most relevant states in the process of moving hydrogen

atoms from the Pd nanoparticle towards the carbon substrate along a minimum energy path, MEP. Those energies are shown in Fig. 7. The upper panel shows first the energy of the reference system formed by Pd₁₃ supported on graphene and a free H₂ molecule. The state of the dissociated hydrogen molecule adsorbed on the metal nanoparticle is 1.4 eV more stable than the reference state. This result is consistent with the occurrence of molecular dissociation in a fraction of the dynamical simulations, as indicated in Table 1. An attempt of displacing one of the H atoms from the nanoparticle to a location on the graphene layer adjacent to the Pd nanoparticle results in jumps of the H atoms back to the metal particle through an intermediate configuration in which the H atom is on top of one of the Pd atoms supported on the graphene layer. The displacement of H to a slightly farther location, still near the Pd nanoparticle, is an endothermic process that requires a substantial energy of 1.9 eV, and the diffusion of H on the graphene surface in the neighborhood of the Pd nanoparticle requires an additional energy of 0.7 eV. The diffusion barrier of H to reach more distant positions from the nanoparticle is even higher, about 1.2 eV on clean graphene⁴⁹. Thus the energy barrier that has to be overcome by the H to spill from the nanoparticle to a distant position on the graphene layer is at least 2.6 eV. A similar picture of events is obtained for the case when the hydrogen molecule dissociates on a supported Pd₁₃ cluster containing six dissociated molecules, that is, twelve H atoms (see lower panel of Fig. 7). Notice that in this latter case, the Pd nanoparticle becomes fully saturated with dissociatively adsorbed hydrogen. Even if the stabilization of the additional dissociated molecule is low compared to the case of the clean Pd particle, the displacement of one H atom towards the graphene substrate again results very unfavorable, and the energies required to displace the H atom to positions near to and far from the Pd particle are 1.9 and 2.1 eV, respectively. The diffusion barrier of H on graphene has not been considered here, and therefore should be added to the latter value. Consequently, this steep uphill motion of the H atoms opposes the spillover and, in agreement with the dynamical simulations discussed above, hydrogen spillover is not expected to occur at room temperature for any degree of hydrogen

saturation of the Pd nanoparticle. Moreover, one should notice that the energy level of the configuration with one H atom spilt onto the graphene support is well above the energy level for desorption of one hydrogen molecule, labelled as “free H₂” in Fig. 7 for both cases. Therefore, increasing the temperature of the system would lead to hydrogen desorption rather than to facilitate H spillover onto the graphene support. In conclusion, both static and dynamical calculations show clear evidence that the spillover of hydrogen does not take place under the conditions investigated in this manuscript and suggest that a critical evaluation of the spillover mechanism under more general conditions is also needed.

4 Conclusions

In summary, we have performed ab initio molecular dynamics simulations of the deposition of molecular hydrogen on palladium nanoparticles supported on graphene, a good model for the pore walls of nanoporous carbon. In order to elucidate how the adsorption and the possible subsequent transfer of H onto the graphene layer depends on the Pd cluster size and on the presence of preadsorbed H, our simulations are performed for clean Pd₆ and Pd₁₃ clusters, as well as for the H-covered Pd₆H₆ and Pd₁₃H₁₂. Dissociation of the hydrogen molecule only occurs on the clean nanoparticles. The fraction of this event is sensitive to -and actually increases with- the nanoparticle size. Molecular adsorption is obtained for the four types of Pd nanoparticles considered in this work, although the percentage of this event is significantly smaller on the clean ones. All in all, it is worthy to remark that H spillover from Pd nanoparticles onto the graphene support is a highly endothermic process. The highly relevant outcome of our study is that, in spite of the large number of simulations performed, not a single event of hydrogen spillover to the carbon substrate has been detected. This clearly demonstrates that the spillover of hydrogen does not take place under the conditions investigated in this manuscript. Therefore, our results lead us to conclude that the often used hypothesis of spillover to justify the observed enhancement of hydrogen storage in porous

carbons promoted by the presence of dopant Pd nanoparticles has to be revised.

Acknowledgement

M. B. R., J. I. J. and M. A. acknowledge support by Basque Departamento de Educación, Universidades e Investigación, the University of the Basque Country UPV/EHU (Grant No. IT-756-13) and the Spanish Ministerio de Economía y Competitividad (Grant No. FIS2013-48286-C2-2-P). J. A. A. and M. J. L. acknowledge support by MINECO (Grant No. MAT2014-54378-R) and Junta de Castilla y León (Grant No. VA050U14). The authors thankfully acknowledge the computer resources provided by the DIPC computing center.

References

- (1) *Fuel Cell Handbook, 7th ed.*; EG&G Technical Services, Inc., US DOE: Morgantown, West Virginia, 2004.
- (2) Jena, P. Materials for Hydrogen Storage: Past, Present, and Future. *J. Phys. Chem. Lett.* **2011**, *2*, 206–211.
- (3) Cabria, I.; López, M. J.; Alonso, J. A. In *Handbook of Nanophysics, Vol. 5 (Functional Materials)*; Sattler, K., Ed.; CRC Press: Boca Ratón, FL, 2010; p 41.1.
- (4) Alonso, J. A.; Cabria, I.; López, M. J. Simulation of hydrogen storage in porous carbons. *J. Mater. Res.* **2013**, *28*, 589–604.
- (5) Wong-Foy, A. G.; Matzger, A. J.; Yaghi, O. M. Exceptional H₂ Saturation Uptake in Microporous Metal-Organic Frameworks. *J. Am. Chem. Soc.* **2006**, *128*, 3494–3495.
- (6) Langmi, H.; Walton, A.; Al-Mamouri, M.; Johnson, S.; Book, D.; Speight, J.; Edwards, P.; Gameson, I.; Anderson, P.; Harris, I. Hydrogen adsorption in zeolites A, X, Y and RHO. *J. Alloys Compd.* **2003**, *356-357*, 710 – 715, Proceedings of the Eighth

International Symposium on Metal-Hydrogen Systems, Fundamentals and Applications (MH2002).

- (7) Mao, W. L.; Mao, H.-k.; Goncharov, A. F.; Struzhkin, V. V.; Guo, Q.; Hu, J.; Shu, J.; Hemley, R. J.; Somayazulu, M.; Zhao, Y. Hydrogen Clusters in Clathrate Hydrate. *Science* **2002**, *297*, 2247–2249.
- (8) McKeown, N. B.; Budd, P. M.; Book, D. Microporous Polymers as Potential Hydrogen Storage Materials. *Macromol. Rapid Commun.* **2007**, *28*, 995–1002.
- (9) Targets for Onboard Hydrogen Storage Systems for Light-duty Vehicles (US DOE, 2009). http://energy.gov/sites/prod/files/2015/01/f19/fcto_myrrdd_table_onboard_h2_storage_systems_doe_targets_ldv.pdf.
- (10) Züttel, A. Materials for hydrogen storage. *Mater. Today* **2003**, *6*, 24 – 33.
- (11) Yushin, G.; Dash, R.; Jagiello, J.; Fischer, J.; Gogotsi, Y. Carbide-Derived Carbons: Effect of Pore Size on Hydrogen Uptake and Heat of Adsorption. *Adv. Funct. Mater.* **2006**, *16*, 2288–2293.
- (12) Jordá-Beneyto, M.; Suárez-García, F.; Lozano-Castelló, D.; Cazorla-Amorós, D.; Linares-Solano, A. Hydrogen storage on chemically activated carbons and carbon nano-materials at high pressures. *Carbon* **2007**, *45*, 293 – 303.
- (13) Patchkovskii, S.; Tse, J. S.; Yurchenko, S. N.; Zhechkov, L.; Heine, T.; Seifert, G. Graphene nanostructures as tunable storage media for molecular hydrogen. *Proc. Natl. Acad. Sci. USA* **2005**, *102*, 10439–10444.
- (14) Peng, L.; Morris, J. R. Prediction of Hydrogen Adsorption Properties in Expanded Graphite Model and in Nanoporous Carbon. *J. Phys. Chem. C* **2010**, *114*, 15522–15529.

- (15) Cabria, I.; López, M.; Alonso, J. Simulation of the hydrogen storage in nanoporous carbons with different pore shapes. *Int. J. Hydrogen Energy* **2011**, *36*, 10748 – 10759.
- (16) Martínez-Mesa, A.; Yurchenko, S. N.; Patchkovskii, S.; Heine, T.; Seifert, G. Influence of quantum effects on the physisorption of molecular hydrogen in model carbon foams. *J. Chem. Phys.* **2011**, *135*, 214701.
- (17) Peng, L. J.; Morris, J. R. Structure and hydrogen adsorption properties of low density nanoporous carbons from simulations. *Carbon* **2012**, *50*, 1394 – 1406.
- (18) Chen, P.; Wu, X.; Lin, J.; Tan, K. L. High H₂ Uptake by Alkali-Doped Carbon Nanotubes Under Ambient Pressure and Moderate Temperatures. *Science* **1999**, *285*, 91–93.
- (19) Yang, R. T. Hydrogen storage by alkali-doped carbon nanotubes-revisited. *Carbon* **2000**, *38*, 623 – 626.
- (20) Bhat, V. V.; Contescu, C. I.; Gallego, N. C.; Baker, F. S. Atypical hydrogen uptake on chemically-activated, ultramicroporous carbon. *Carbon* **2010**, *48*, 1331 – 1340.
- (21) Contescu, C. I.; van Benthem, K.; Li, S.; Bonifacio, C. S.; Pennycook, S. J.; Jena, P.; Gallego, N. C. Single Pd atoms in activated carbon fibers and their contribution to hydrogen storage. *Carbon* **2011**, *49*, 4050 – 4058.
- (22) Lueking, A. D.; Yang, R. T. Hydrogen spillover to enhance hydrogen storage-study of the effect of carbon physicochemical properties. *Appl. Catal. A-Gen* **2004**, *265*, 259 – 268.
- (23) Yoo, E.; Gao, L.; Komatsu, T.; Yagai, N.; Arai, K.; Yamazaki, T.; Matsuishi, K.; Matsumoto, T.; Nakamura, J. Atomic Hydrogen Storage in Carbon Nanotubes Promoted by Metal Catalysts. *J. Phys. Chem. B* **2004**, *108*, 18903–18907.

- (24) Zacharia, R.; Kim, K. Y.; Kibria, A. F.; Nahm, K. S. Enhancement of hydrogen storage capacity of carbon nanotubes via spill-over from vanadium and palladium nanoparticles. *Chem. Phys. Lett.* **2005**, *412*, 369 – 375.
- (25) Anthony J. Lachawiec, J.; Qi, G.; Yang, R. T. Hydrogen Storage in Nanostructured Carbons by Spillover: Bridge-Building Enhancement. *Langmuir* **2005**, *21*, 11418–11424, PMID: 16285820.
- (26) Kim, B.-J.; Lee, Y.-S.; Park, S.-J. Preparation of platinum-decorated porous graphite nanofibers, and their hydrogen storage behaviors. *J. Colloid Interf. Sci.* **2008**, *318*, 530 – 533.
- (27) Parambath, V. B.; Nagar, R.; Ramaprabhu, S. Effect of Nitrogen Doping on Hydrogen Storage Capacity of Palladium Decorated Graphene. *Langmuir* **2012**, *28*, 7826–7833, PMID: 22548388.
- (28) Conner, W. C.; Falconer, J. L. Spillover in Heterogeneous Catalysis. *Chem Rev.* **1995**, *95*, 759–788.
- (29) Cheng, H.; Chen, L.; Cooper, A. C.; Sha, X.; Pez, G. P. Hydrogen spillover in the context of hydrogen storage using solid-state materials. *Energy Environ. Sci.* **2008**, *1*, 338–354.
- (30) Chen, L.; Cooper, A. C.; Pez, G. P.; Cheng, H. Mechanistic study on hydrogen spillover onto graphitic carbon materials. *J. Phys. Chem. C* **2007**, *111*, 18995–19000.
- (31) Singh, A. K.; Ribas, M. A.; Yakobson, B. I. H-Spillover through the Catalyst Saturation: An Ab Initio Thermodynamics Study. *ACS Nano* **2009**, *3*, 1657–1662, PMID: 19534542.
- (32) López, M. J.; Cabria, I.; Alonso, J. A. Simulated porosity and electronic structure of nanoporous carbons. *J. Chem. Phys.* **2011**, *135*, 104706.

- (33) Parambath, V. B.; Nagar, R.; Sethupathi, K.; Ramaprabhu, S. Investigation of Spillover Mechanism in Palladium Decorated Hydrogen Exfoliated Functionalized Graphene. *J. Phys. Chem. C* **2011**, *115*, 15679–15685.
- (34) Kresse, G.; Furthmüller, J. Efficiency of ab-initio total energy calculations for metals and semiconductors using a plane-wave basis set. *Comput. Mater. Sci.* **1996**, *6*, 15 – 50.
- (35) Kresse, G.; Hafner, J. Ab initio molecular dynamics for liquid metals. *Phys. Rev. B* **1993**, *47*, 558–561.
- (36) Perdew, J. P.; Chevary, J. A.; Vosko, S. H.; Jackson, K. A.; Pederson, M. R.; Singh, D. J.; Fiolhais, C. Atoms, molecules, solids, and surfaces: Applications of the generalized gradient approximation for exchange and correlation. *Phys. Rev. B* **1992**, *46*, 6671–6687.
- (37) Kresse, G.; Joubert, D. From ultrasoft pseudopotentials to the projector augmented-wave method. *Phys. Rev. B* **1999**, *59*, 1758–1775.
- (38) Monkhorst, H. J.; Pack, J. D. Special points for Brillouin-zone integrations. *Phys. Rev. B* **1976**, *13*, 5188–5192.
- (39) Methfessel, M.; Paxton, A. T. High-precision sampling for Brillouin-zone integration in metals. *Phys. Rev. B* **1989**, *40*, 3616–3621.
- (40) Cabria, I.; López, M. J.; Fraile, S.; Alonso, J. A. Adsorption and Dissociation of Molecular Hydrogen on Palladium Clusters Supported on Graphene. *J. Phys. Chem. C* **2012**, *116*, 21179–21189.
- (41) D’Anna, V.; Duca, D.; Ferrante, F.; Manna, G. L. DFT studies on catalytic properties of isolated and carbon nanotube supported Pd₉ cluster-I: adsorption, fragmentation and diffusion of hydrogen. *Phys. Chem. Chem. Phys.* **2009**, *11*, 4077–4083.

- (42) Barone, G.; Duca, D.; Ferrante, F.; Manna, G. L. CASSCF/CASPT2 Analysis of the Fragmentation of H₂ on a Pd₄ Cluster. *Int. J. Quantum Chem.* **2010**, *110*, 558–562.
- (43) Dacapo, See <https://wiki.fysik.dtu.dk/dacapo> for a description of the total energy code, based on the density functional theory. 2009.
- (44) Vanderbilt, D. Soft Self-Consistent Pseudopotentials in a Generalized Eigenvalue Formalism. *Phys. Rev. B* **1990**, *41*, R7892.
- (45) Mushrif, S. H.; Rey, A. D.; Peslherbe, G. H. Energetics and dynamics of hydrogen adsorption, desorption and migration on a carbon-supported palladium cluster. *J. Mater. Chem.* **2010**, *30*, 10503–10510.
- (46) Yang, R. T.; Wang, Y. Catalyzed Hydrogen Spillover for Hydrogen Storage. *J. Am. Chem. Soc.* **2009**, *131*, 4224–4226.
- (47) Chen, H.; Wang, L.; Yang, J.; Yang, R. T. Investigation on Hydrogenation of MetalOrganic Frameworks HKUST-1, MIL-53, and ZIF8 by Hydrogen Spillover. *J. Phys. Chem. C* **2013**, *117*, 7565–7576.
- (48) Wang, L.; Lachawiec Jr., A. J.; Yang, R. T. Nanostructured adsorbents for hydrogen storage at ambient temperature: high-pressure measurements and factors influencing hydrogen spillover. *RSC Adv.* **2013**, *3*, 23935.
- (49) Lueking, A. D.; Psfogiannakis, G.; Froudakis, G. E. Atomic Hydrogen Diffusion on Doped and Chemically Modified Graphene. *J. Phys. Chem. C* **2013**, *117*, 6312–6319.

Graphical TOC Entry

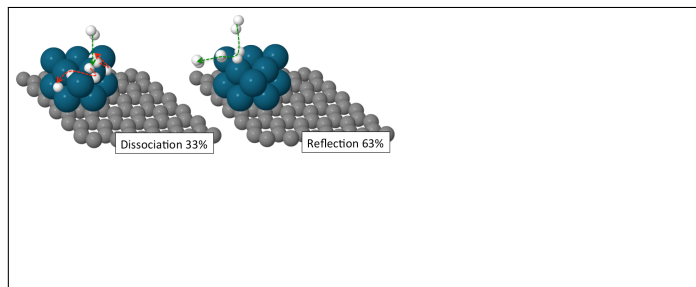


Table 1: Number of trajectories that lead to dissociation (ND), non-dissociative molecular adsorption (NA) and reflection (NR) for H_2 molecules incident on different Pd nanoparticles. The number of simulations for each nanoparticle is 60. NP is the number of pathological trajectories (see text).

Particle	ND	NA	NR	NP
Pd_6	3	13	43	1
Pd_{13}	20	2	38	0
Pd_6H_6	0	26	32	2
$\text{Pd}_{13}\text{H}_{12}$	0	12	42	3

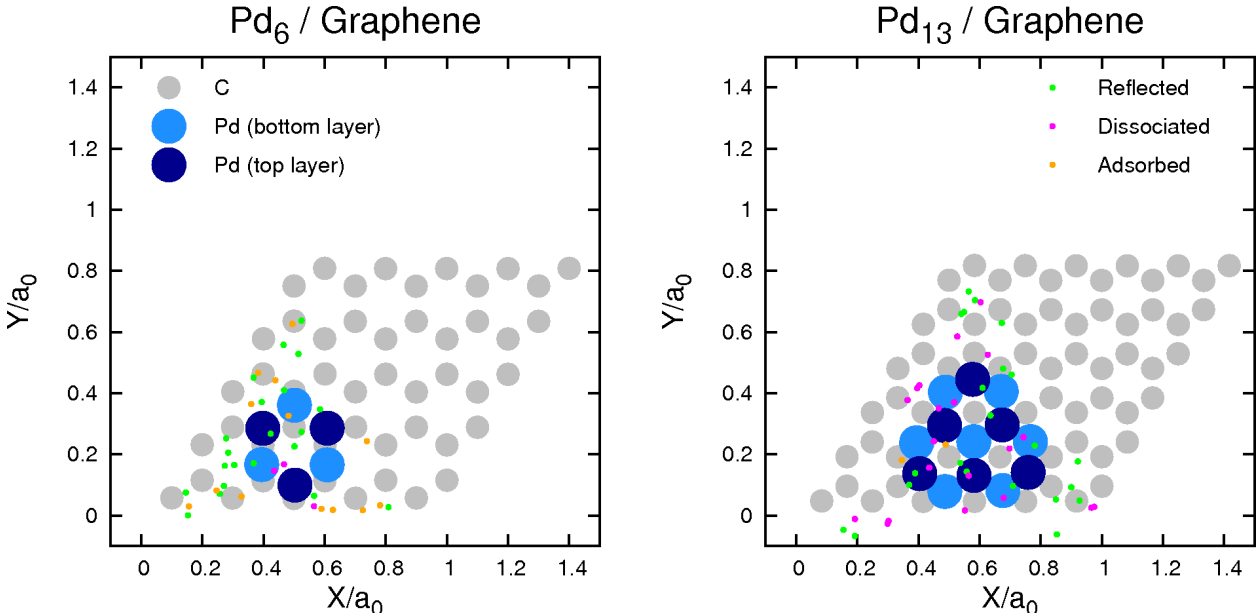


Figure 1: Initial lateral coordinates of the H_2 molecule in the AIMD simulations. The panels show a top view of the supercells used to represent the Pd_6 and Pd_{13} nanoparticles supported on graphene. The positions are given in fractional coordinates (a_0 is the hexagonal lattice parameter). The C and Pd atoms are represented by medium gray and large blue circles, respectively. The small colored dots indicate the initial coordinates (X, Y) of the H_2 molecule center of mass in the AIMD simulations. The dot colors account for the incidence conditions that give rise to reflection (green), dissociation (magenta), and adsorption (orange).

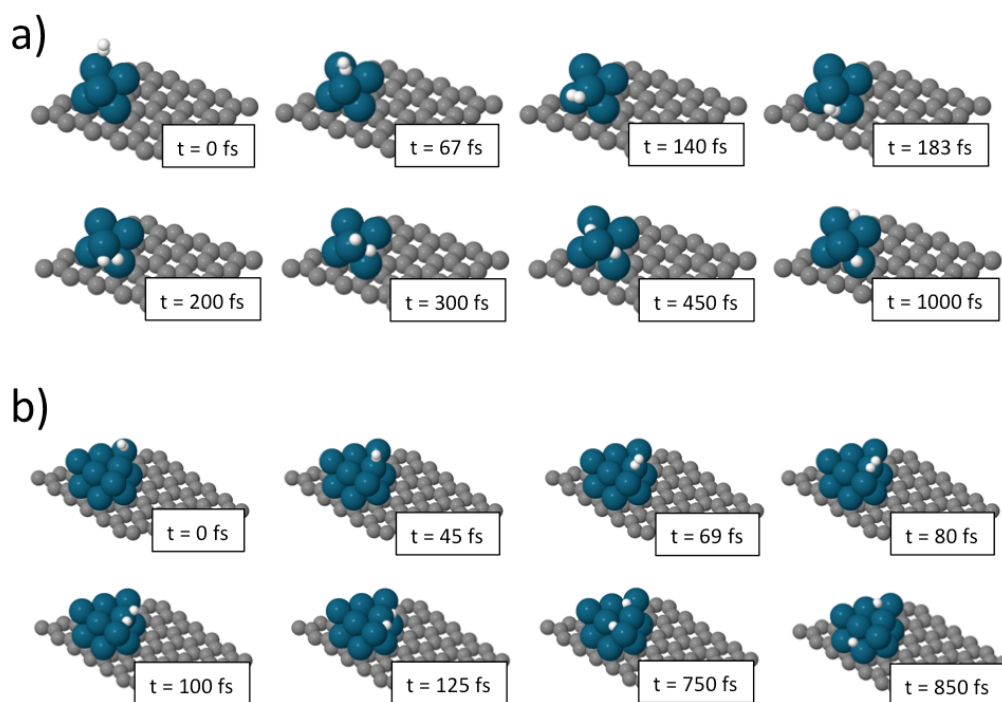


Figure 2: Snapshots of representative trajectories leading to dissociation for a H_2 molecule incident on a (a) Pd_6 and a (b) Pd_{13} nanoparticle supported on a graphene monolayer. White spheres correspond to the H atoms, blue spheres to the Pd atoms, and grey spheres to the C atoms.

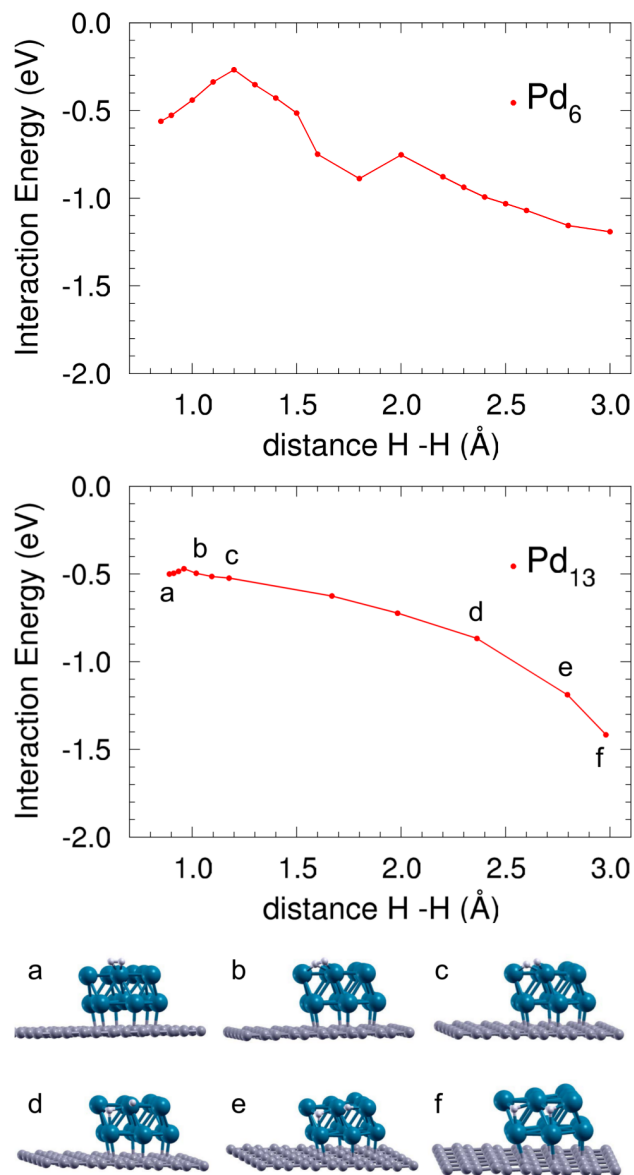


Figure 3: Interaction energy of H_2 with supported Pd_{13} (second panel) along a minimum energy path for hydrogen dissociation. The initial configuration (a) corresponds to the adsorbed hydrogen molecule, and the final configuration (f) corresponds to dissociated hydrogen. Selected configurations along the path, labeled from (b) to (e), are also shown. The dissociation barrier of H_2 on supported Pd_6 (first panel) is given for comparison.

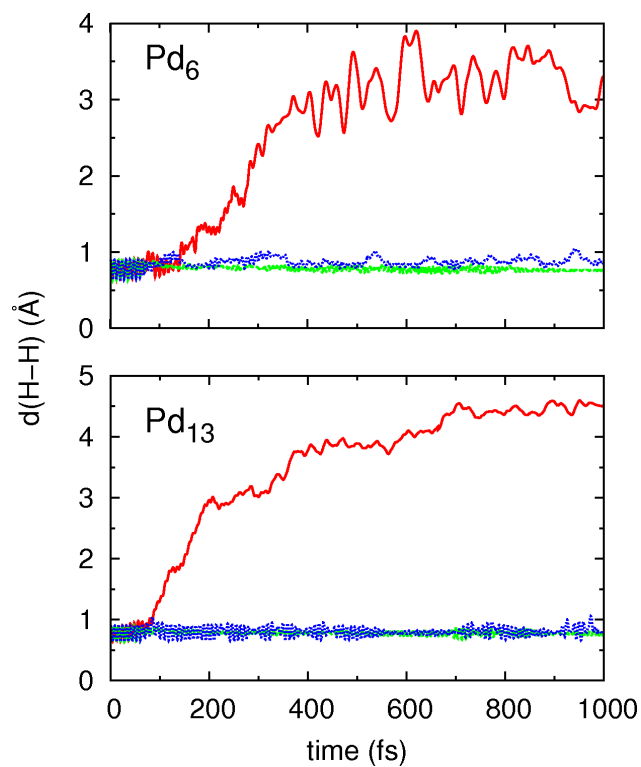


Figure 4: Time dependence of the average internuclear distance between the H atoms of the H_2 molecules impinging on the supported Pd_6 and Pd_{13} nanoparticles. The red curves correspond to the dissociated molecules, the green curves to the reflected molecules, and the blue curves to the non-dissociatively adsorbed molecules.

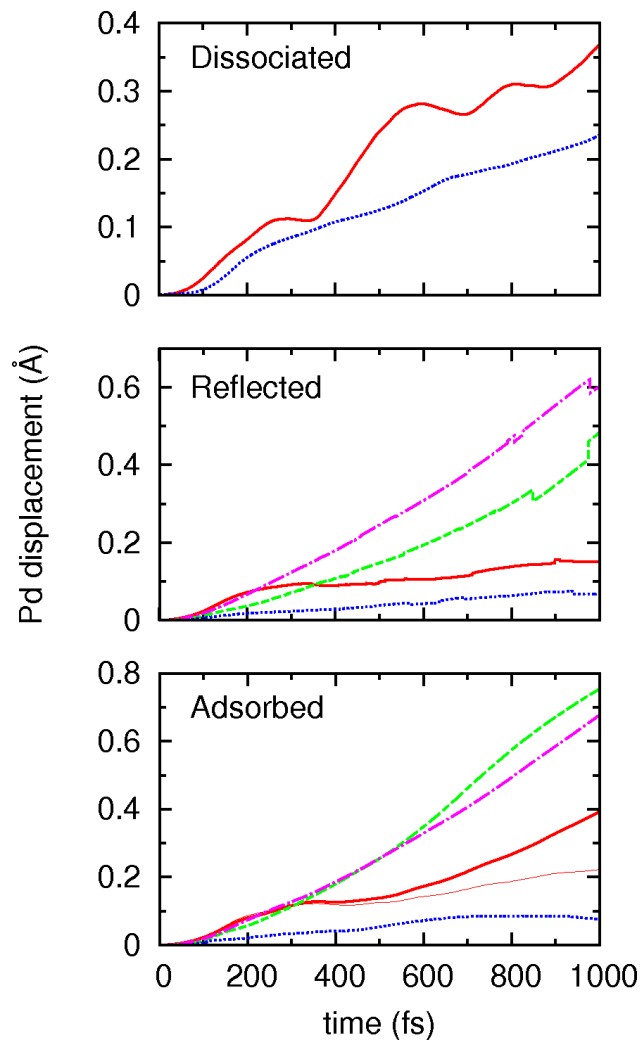


Figure 5: Time dependence of the average displacement of the Pd atoms upon their interaction with the incoming H_2 molecule. The three panels correspond to different outcomes of the trajectories (dissociation, reflection and non-dissociative adsorption) as labeled. Thick solid red curves show the results for Pd_6 , dotted blue curves for Pd_{13} , dashed green curves for Pd_6H_6 , and dotted-dashed magenta curves for $\text{Pd}_{13}\text{H}_{12}$. In the case of adsorbed molecules, the thin solid red curve is obtained by removing from the calculation the trajectories in which the Pd_6 rotates.

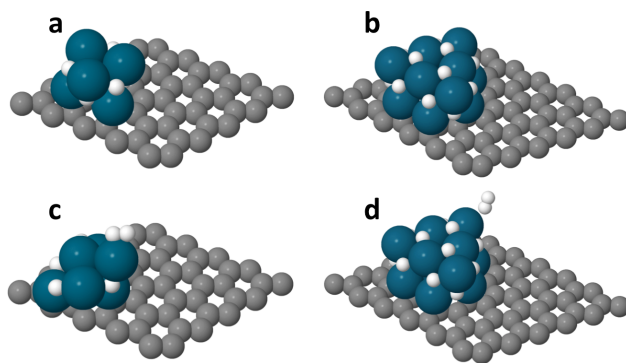


Figure 6: Panels (a) and (b) show the configurations of the relaxed Pd_6H_6 and $\text{Pd}_{13}\text{H}_{12}$, respectively, before starting the AIMD simulations. Panels (c) and (d) show, respectively, the configuration adopted by the Pd_6H_6 and $\text{Pd}_{13}\text{H}_{12}$ nanoparticles at the end of the simulation time (1 ps) for two selected trajectories in which molecular adsorption occurs.

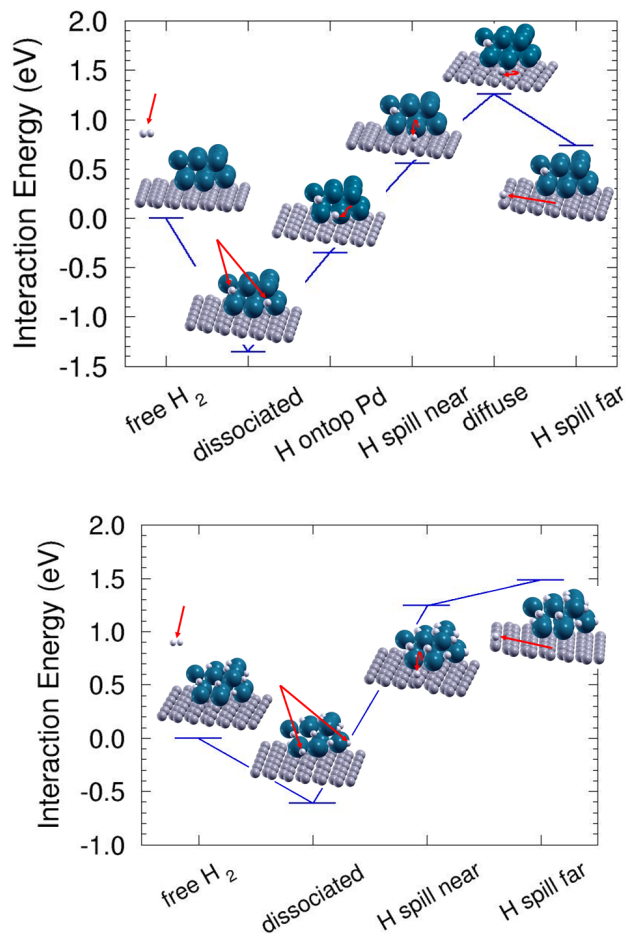


Figure 7: Upper panel: Representative energies, along a minimum energy path MEP of the process of H spillover (indicated by arrows) onto the graphene support from Pd₁₃ with one dissociatively adsorbed hydrogen molecule. The energies for the dissociative adsorption of the hydrogen molecule on the Pd nanoparticle are also given. Lower panel: the same information is given for Pd₁₃ with seven dissociatively adsorbed hydrogen molecules. This case corresponds to the full saturation of the Pd nanoparticle with dissociated hydrogen. The energies for the dissociative adsorption of one hydrogen molecule on the Pd nanoparticle with six preadsorbed hydrogen molecules are also given.